09,12

Hybrid spherical microresonators with luminescent organic dyes FITC and DCM

© A.A. Dukin, D.A. Eurov, E.Yu. Stovpiaga, A.N. Smirnov, D.A. Kurdyukov, V.G. Golubev

Ioffe Institute,
St. Petersburg, Russia

E-mail: dookin@gvg.ioffe.ru

Received April 4, 2023
Revised April 4, 2023
Accepted April 16, 2023

Luminescent hybrid spherical microresonators of two types consisting of monodisperse spherical silica particles with a diameter of 3.5 μm coated with either FITC dye molecules or a 200 nm thick mesoporous silica shell containing DCM dye are fabricated. The luminescence spectra of microresonators are studied and the experimental emission spectra are simulated using the method of spherical wave transfer matrices. The ratio of intensities of emission lines into whispering gallery modes with different polarizations and the same polar and radial indices is analyzed. It is shown that the ratio depends on the orientation of the dipole moment of the radiative transition of dye molecules relative to the surface of spherical silica particles.

Keywords: spherical microresonator, whispering gallery modes, organic dyes, photoluminescence.

DOI: 10.21883/PSS.2023.06.56118.52

1. Introduction

Spherical microresonators (SMR) have unique optical properties and are in the spotlight in different areas of optics [1–7]. Their properties are based on whispering-gallery modes (WGM) — a special type of eigenmodes of the electromagnetic field of a microsphere. WGM feature high Q-factor and low effective volume. Electromagnetic field of WGM is localized near the SMR surface and partially penetrates the environment exerting influence on spontaneous emission of light-emitting material on the SMR surface. Light-emitting materials and particles may be, for example, attached to the microsphere surface or introduced into its shell.

SMR is used as basis for hybrid light-emitting structures where quantum dots [8], J-aggregates [9], MoS_2 [10], carbon nanodots [11], diamond nanocrystals with color centers [12] are coupled with the microspheres. Such hybrid structures may be used for detecting environmental variables, chemical and biological substances, etc. [13,14].

Organic dyes such as fluorescein isothiocyanate (FITC) [15] and 4-dicyanomethylene-2-methyl-6-(p-(dimethyloamino)styryl)-4H-pyran (DCM) are promising luminescent materials used to create new hybrid light-emitting structures. They have a wide visible luminescence spectrum, high quantum efficiency and are extensively used as phosphors [16].

For the purpose of this study, two types of light-emitting hybrid spherical microresonators (HSMR) were prepared and consist of monodisperse spherical optically-transparent silica particles covered either by FITC molecules or mesoporous DCM-containing silica shell. HSMR luminescence spectra were studied and experimental spectra simulation was carried out for the studied structures.

Due to interaction between the WGM electromagnetic field and electronic excitations of FITC and DCM molecules in the spontaneous emission spectrum of dyes, a series of narrow peaks occurs whose positions coincide with the HSMR whispering-gallery modes. The WGM wave length depends heavily on the refraction index of the environment, optical and geometrical parameters of HSMR. This offers the possibility of creating luminescent sensors of chemical and biological substances, temperature, pressure, environment refraction index, etc., on the basis of HSMR [13]. A wide emission spectrum of organic dyes allows simultaneous recording and analysis of a set of photoluminescence lines (PL) corresponding to WGM to improve biological substance detection efficiency [14]. HSMR with luminescent organic dyes may be used as sensors introduced directly into a living cell, because the optical signal will be excited and detected remotely.

2. Preparing hybrid spherical microresonators with luminescent organic dyes

Spherical silica particles (a-SiO_2) were synthesized by base hydrolysis of tetraethoxysilane (TEOS) in alcohol-water-ammonia fluid [17,18]. Initially, 700 ± 25 nm particles were obtained. Then „completion of growing“ [18] was carried out as follows. In the reaction mixture with equivalent composition containing the prepared 700 nm silica particles, portions of TEOS were added with equal time intervals. As a result of TEOS hydrolysis, the initial particles were coated with a hydrated a-SiO_2 layer leading

to growth of particles (increase in diameter). At the last stage, the synthesized particles were annealed in air at 500°C. Finally, spherical silica particles $3.5 \pm 0.15\,\mu$m in diameter were produced.

Functionalization of the spherical silica particle surfaces with FITC dye was carried out in two stages. At the first stage, the silica surface was modified with NH_2-groups by aminopropyltriethoxysilane adsorption from its toluene solution during 24 hours. Then the particles were annealed at 100°C during 2 h. At the second stage, FITC chemisorption from its alcohol solution was carried out. Then the particles were separated by centrifuging and washed with deionized water to remove the nonspecifically bonded FITC. The remaining FITC molecules were chemically bonded with the microsphere surfaces via N=C=S-group.

DCM (Sigma-Aldrich) dye was another luminescent material used for the research. This is a high effective dye [19] which is widely used in various liquid systems (solvents) and solid matrices. Disadvantage of the chosen dye are its strongly pronounced mutagenic properties [20]. In addition, [21] shows that properties of the solvent containing the dye (e.g. solvent polarity) may have a considerable impact on the DCM absorption and luminescence spectra. Therefore, this study offers an approach that involves mesoporous silica shell impregnation with DCM. Silica used as a matrix for DCM is known to increase photostability of DCM [22]. The presence of the dye inside the shell, on the one hand, minimizes adverse environmental impact of DCM and, on the other hand, prevents degradation of the DCM emission properties due to the environmental influence.

The initial particles were coated with mesoporous a-SiO_2 shell using a procedure similar to the mesoporous silica particle synthesis [23]. For this, the intial a-SiO_2 particles were dispersed in alcohol-water-ammonia fluid containing a pore-forming agent — cetyltrimethyl ammonium bromide (CTAB) and DCM. TEOS was added to the obtained solution drop by drop with stirring. Synthesis time was 6 h, then the obtained particles were separated by centrifuging and then dried. Mixture composition and synthesis conditions enabled mesoporous silica shells of uniform thickness to be applied to the particles. It was found that addition of dye into the reaction mixture had no influence on the mesoporous silica formation mechanism. DCM molecules like rhodamine molecules [24] are probably built in the silica structure during synthesis. As a result, the obtained particles representing a nonporous a-SiO_2 core coated with a 200 nm mesoporous silica shell impregnated with DCM dye and CTAB.

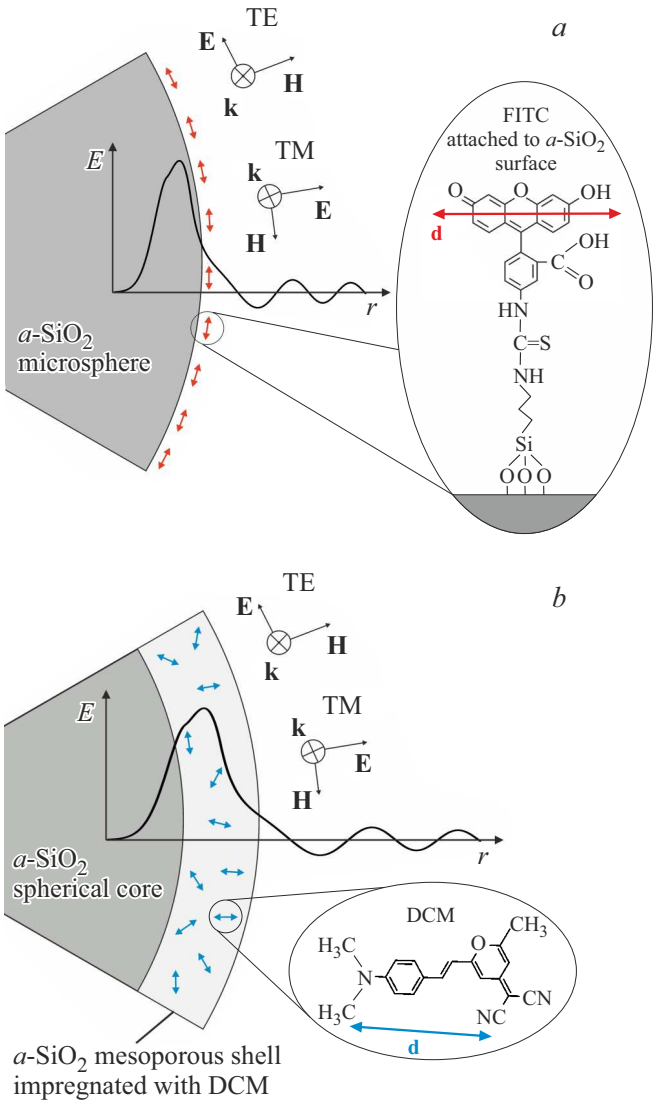

Figure 1. Schematic diagram of a cross-section segment *a*) HSMR−FITC and *b*) HSMR−DCM. Small double-headed arrows near the microsphere surface (*a*) and inside the shell (*b*) show the emitting dipole moment orientation of the FITC (*a*) and DCM (*b*) molecules. Details: structure of the FITC molecule attached to the microsphere surface (*a*), DCM molecule in pores (*b*) and orientation of dipole emitting moment vector **d** of these molecules. Both figures show electric field vectors **E**, magnetic field vectors **H** and wave vector **k** for TE- and TM-polarized WGM and a curve showing typical distribution of electric field strength E over the radial coordinate r for TE-polarized WGM with $q = 1$.

3. Results and discussion

HSMR is emitted into WGM which are described by spherical waves and characterized by three numbers: polar index l ($l \geq 1$), azimuthal index m ($m = l$ or m close to l), radial index q ($q \geq 1$) and two polarizations (TE and TM). Polar index l and azimuthal index m describe the angular field distribution (the number of mode maxima in the equatorial section is $2|m|$, the number of mode maxima in the meridional section is $l - |m| + 1$). Radial index q corresponds to the number of the mode maxima lying within HSMR along the radius. For TE-polarized WGM, the electric field vector is parallel to the HSMR outer surface, for TM-polarized WGM, the electric field vector is almost perpendicular to the HSMR outer surface (Figure 1). WGM

will be denoted hereinafter as TE_l^q or TM_l^q, where TE and TM are WGM polarizations, q and l are the corresponding indices. Within HSMR, the WGM field is pressed against the outer surface in the form of a narrow equatorial ring. Outside HSMR, not far from the surface, the WGM field decays exponentially (evanescent field region).

The HSMR emission spectra, radial field distribution and WGM parameters (wavelength, polarization, polar and radial indices) are calculated using the electromagnetic wave field expansion in the basis of vector spherical harmonics and the method of spherical wave transfer matrices [25]. For this, condition of tangential component continuity of the electric and magnetic fields at the shell boundaries and on the microsphere surface was used. For fitting the calculated WGM wavelengths to the experimental wavelengths, diameter of a-SiO_2 microsphere, thickness and refraction index of a-SiO_2 mesoporous shell filled with CTAB and DCM were varied.

In the calculated spectrum, the dipole emission intensity on the microsphere surface and within the shell is normalized to the dipole emission intensity in homogeneous medium whose relative dielectric and magnetic permittivities are equal to those for the medium on the microsphere surface (for HSMR–FITC) or within the shell (for HSMR–DCM). The calculated HSMR emission spectrum contains many pairs of narrow peaks, that correspond to the emission in WGM with the same l and $q = 1$, but with different TE and TM polarization [25]. For more details of the calculation procedure, refer to [26].

Figures 1, *a* and *b* show the schematic diagram of a cross-section segment HSMR–FITC and HSMR–DCM. Near the outer boundary of HSMR, electric field vectors **E**, magnetic field vectors **H** and wave vector **k** are shown for TE- and TM-polarized WGM. Typical distribution of the electric field strength along the radial coordinate for the TE-polarized WGM with $q = 1$ is also shown. This has a wide maximum within the microsphere (Figure 1, *a*) or within the shell (Figure 1, *b*) and a small evanescent field region outside the outer boundary of HSMR. In HSMR–FITC, dye molecules are attached to the microsphere surface and interact with the WGM evanescent field (Figure 1, *a*). Size of the FITC molecule is approximately 1.5 nm, and the evanescent field region size, according to the calculations, is equal to 310–390 nm, therefore the FITC molecules are completely within this region. In HSMR–DCM, DCM molecules are in the pores within the shell and interact with the WGM travelling wave field; whereby a considerable portion and maximum of the WGM field are within the shell (Figure 1, *b*).

Luminescence of dye molecules such as FITC and DCM is described by a dipole moment of the emission transition [16,27]. Dipole moment vectors of the dye molecules are shown by small double-headed arrows on the surface of HSMR–FITC microsphere (Figure 1, *a*) and within HSMR–DCM shell (Figure 1, *b*). Near the HSMR section, enlarged structures of the FITC molecule attached to the surface of a-SiO_2 microsphere (Figure 1, *a*) and of the DCM molecule in the shell pores (Figure 1, *b*) are shown and orientation of emission transition dipole moment vector **d** with respect to the molecule structure is specified.

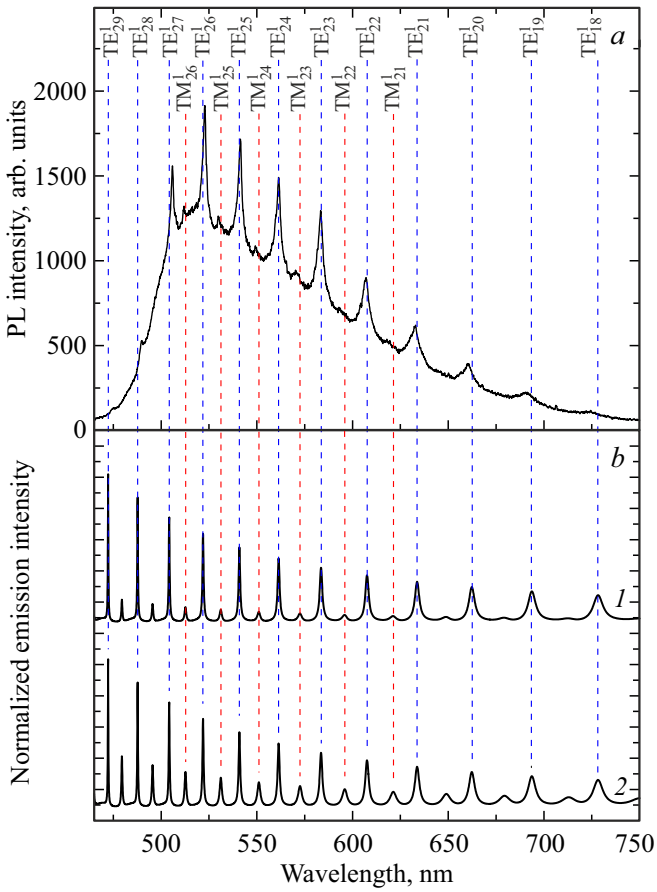

Figure 2. *a*) Experimental PL spectrum of the hybrid spherical microresonator with FITC. The excitation wavelength is $\lambda = 442$ nm. Vertical dashed lines show the specified WGM positions. *b*) Calculated emission spectrum of HSMR–FITC, *1* — emitting dipoles are oriented parallel to the surface, *2* — emitting dipoles are oriented in all directions with the equal probability.

The study investigates the HSMR PL spectra at room temperature using Horiba Jobin Yvon T64000 spectrometer equipped with confocal microscope. As an excitation source, 442 nm He–Cd laser and 532 nm Nd:YAG laser were used.

Figure 2, *a* shows the experimental photoluminescence spectrum of HSMR–FITC. A series of narrow large-amplitude peaks between which lower amplitude peaks are located can be seen against a wide band in the spectrum. Figure 2, *b* shows the calculated emission spectrum of this HSMR for two cases: when emitting dipoles are oriented parallel to the microsphere surface (curve *1*) and when they are oriented in all directions with equal probability (curve *2*). Comparison with the calculated spectra (Figure 2, *b*) allowed to identify the observed peaks in the PL spectrum as the FITC emission lines in

WGM with TE-polarization (large-amplitude peaks) and with TM-polarization (small-amplitude peaks) and to find the polar and radial indices of the corresponding modes.

In the experimental spectrum, the amplitude of TE-polarized peaks is much higher than that of TM-polarized peaks for WGM with the same l and q. This may be explained by the orientation of the emission transition dipole moment vector of the FITC molecule. A FITC molecule with the maximum intensity emits into those electromagnetic field modes whose electric field vector is parallel to the dipole moment vector and does not emit in those modes whose electric field vector is perpendicular to the dipole moment vector. If the emitting dipoles of the FITC molecules on the microsphere surface are oriented in all directions with equal probability, then emission is performed both into TE-polarized WGM whose electric field vector is parallel to the HSMR surface and into TM-polarized WGM whose electric field vector is almost perpendicular to the HSMR surface. Influence of the dipole orientation on the PL spectrum is supported by calculations of the HSMR−FITC emission spectrum when the emitting dipoles of FITC molecules are parallel to the microsphere surface (Figure 2, *b*, curve *1*) and when they are oriented in all directions with equal probability (Figure 2, *b*, curve *2*). With dipole orientation in all directions, the ratio of peak amplitudes corresponding, for example, to polarized modes TE^1_{25} and TM^1_{25} with equal indices in the calculated spectrum (Figure 2, *b*, curve *2*) is equal to 2.6, which is lower that in the experimental spectrum (Figure 2, *a*), where this ratio is 8.1.

In the prepared HSMR, FITC molecules are chemically bonded with the microsphere surface via N=C=S group and, therefore, the xanthene unit is oriented parallel to the HSMR surface (zoomed-in view of the attached FITC molecule is shown in Figure 1, *a*). For FITC, the emission transition dipole moment vector is oriented along the xanthene unit [28–30] and, thus, parallel to the HSMR surface. Due to such orientation, the major portion of the FITC molecule emission is carried out into the TE-polarized WGM where the electric field vector direction is almost the same as the dipole moment vector direction and a much smaller portion of the FITC molecule emission is carried out into the TM-polarized WGM where the electric field vector direction is almost perpendicular to the dipole moment vector. Therefore, the amplitude of TE-peaks is much higher than that of TM-peaks with the same indices. This is supported by the calculation of the dipole layer emission spectrum on the microsphere surface when the dipoles are oriented parallel to the surface (Figure 2, *b*, curve *1*). In the calculated spectrum, the ratio of peak amplitudes with the same indices is approximately the same as that of the experimental spectrum. Such ordered orientation of the FITC molecules allows to reduce the number of WGM lines to be detected in the experimental spectra and, thus, to reduce the eigenmode frequency spectrum density in HSMR.

Figure 3 shows the experimental (*a*) and calculated (*b*) PL spectra of HSMR−DCM. A series of large-amplitude peaks between which lower amplitude peaks are located can

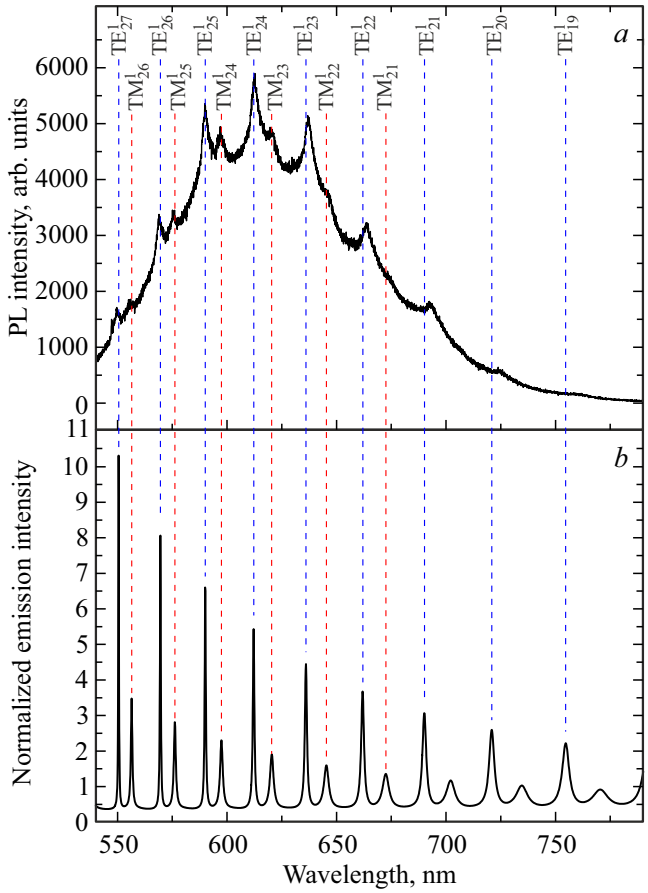

Figure 3. *a*) Experimental PL spectrum of the hybrid spherical microresonator with DCM. The excitation wavelength is $\lambda = 532$ nm. Vertical dashed lines show the specified WGM positions. *b*) Calculated emission spectrum of HSMR−DCM, emitting dipoles are oriented in all directions with the equal probability.

be seen against a wide band in the experimental spectrum. The calculation allowed to fit the WGM wavelengths to the peak maxima wavelengths in the PL spectrum. Thus, all peaks were identified as the DCM emission lines in WGM as well as polarization, polar and radial indices of the corresponding WGM were found. Fitting allowed to clarify the refraction index ($n = 1.438$) and thickness (200.4 nm) of the shell.

For HSMR−DCM, the refraction index of the shell found by way of fitting is a little higher than the refraction index of the core $n = 1.39$. It should be noted that, in the structure where refraction index of the shell is higher than the refraction index of the core, the TE-mode peak amplitude may be several orders of magnitude higher than the TM-mode peak amplitude with the same indices [31]. This may be in fact implemented, if the refraction index of the shell is much higher than the refraction index of the core, and the shell has a subwavelength thickness. With such parameters of the shell, WGM will propagate within the shell as waveguide modes [31].

The DCM dipole moment is oriented approximately along the molecule axis between the end electron-donor (dimethylamine group) and electron-acceptor (pyran ring with two cyano groups) substituents [32] (Figure 1, *b*). DCM molecules are located in the shell pores and oriented randomly against the microsphere surface, therefore the emitting dipole moments of DCM molecules are also oriented in all directions with equal probability. As a result, the ratio of peak amplitudes corresponding to TE- and TM-polarized WGM with the same indices in the experimental spectrum is approximately the same as in the calculated spectrum with random orientation of emitting dipoles.

WGM peaks in the PL spectrum of HSMR−DCM is wider than the WGM peaks in the PL spectrum of HSMR−FITC. This may be explained by additional broadening of WGM in HSMR−DCM due to light scattering on volume inhomogeneities and surface roughness of the mesoporous shell and by broadening due to the influence of possible nonsphericity of the prepared HSMR−DCM.

4. Conclusion

Two types of luminescent hybrid spherical microresonators with organic dyes were prepared herein. Microresonators are composed of monodisperse spherical optically-transparent silica particles 3.5μm in diameter, whose surface is coated with FITC dye molecules or with 200 nm mesoporous silica shell impregnated with DCM dye. Intensive narrow lines associated with the dye emission into the whispering-gallery modes of the microresonators were observed throughout the dye emission wavelength range in the photoluminescence spectra. Comparison with the photoluminescence spectra calculation performed using the method of spherical wave transfer matrices allowed to identify all observed lines. Ratio of intensities for the emission lines into the whispering-gallery modes with different polarization and same polar and radial indices was analyzed. It is shown that the ratio depends on the the orientation of the dipole moment of the radiative transition of dye molecules with respect to the spherical silica particle surfaces.

Funding

The study was carried out using state budget funds on the topic of state assignment 0040-2019-0012.

Conflict of interest

The authors declare that they have no conflict of interest.

References

[1] M.R. Foreman, J.D. Swaim, F. Vollmer. Adv. Opt. Photon. **7**, *2*, 168 (2015).
[2] J. Ward, O. Benson. Laser Photon. Rev. **5**, *4*, 553 (2011).
[3] A. Chiasera, Y. Dumeige, P. Féron, M. Ferrari, Y. Jestin, G. Nunzi Conti, S. Pelli, S. Soria, G.C. Righini. Laser Photon. Rev. **4**, *3*, 457 (2010).
[4] Y.P. Rakovich, J.F. Donegan. Laser Photon. Rev. **4**, *2*, 179 (2010).
[5] G.C. Righini, S. Soria. Sensors **16**, *6*, 905 (2016).
[6] L. Cai, J. Pan, Y. Zhao, J. Wang, S. Xiao. Phys. Status Solidi A **217**, *6*, 1900825 (2020).
[7] D. Venkatakrishnarao, E.A. Mamonov, T.V. Murzina, R. Chandrasekar. Adv. Opt. Mater. **6**, *18*, 1800343 (2018).
[8] C.E. Finlayson, P.J.A. Sazio, R. Sanchez-Martin, M. Bradley, T.A. Kelf, J.J. Baumberg. Semicond. Sci. Technol. **21**, *3*, L21 (2006).
[9] D. Melnikau, D. Savateeva, A. Chuvilin, R. Hillenbrand, Y.P. Rakovich. Opt. Expr. **19**, *22*, 22280 (2011).
[10] Y. Mi, Z. Zhang, L. Zhao, S. Zhang, J. Chen, Q. Ji, J. Shi, X. Zhou, R. Wang, J. Shi, W. Du, Z. Wu, X. Qiu, Q. Zhang, Y. Zhang, X. Liu. Small **13**, *42*, 1701694 (2017).
[11] D.A. Eurov, E.Yu. Stovpiaga, D.A. Kurdyukov, A.A. Dukin, A.N. Smirnov, V.G. Golubev. Phys. Solid State **62**, *10*, 1898 (2020).
[12] S. Schietinger, O. Benson. J. Phys. B **42**, *11*, 114001 (2009).
[13] T. Reynolds, N. Riesen, A. Meldrum, X. Fan, J.M.M. Hall, T.M. Monro, A. François. Laser Photon. Rev. **11**, *2*, 1600265 (2017).
[14] M. Himmelhaus, S. Krishnamoorthy, A. Francois. Sensors **10**, *6*, 6257 (2010).
[15] R. Sjöback, J. Nygren, M. Kubista. Spectrochimica A **51**, *6*, L7 (1995).
[16] J.R. Lakowicz. Principles of Fluorescence Spectroscopy. Springer, Singapore (2006). 954 p.
[17] E.Yu. Trofimova, A.E. Aleksenskii, S.A. Grudinkin, I.V. Korkin, D.A. Kurdyukov, V.G. Golubev. Colloid J. **73**, *4*, 546 (2011).
[18] S.A. Grudinkin, N.A. Feoktistov, E.Yu. Trofimova, D.A. Kurdyukov, K.V. Bogdanov, A.V. Baranov, A.V. Fedorov, V.G. Golubev. Tech. Phys. Lett. **39**, *4*, 341 (2013).
[19] P.R. Hammond. Opt. Commun. **29**, *3*, 331 (1979).
[20] B.J. Wuebbles, J.S. Felton. Environ Mutagen. **7**, *4*, 511 (1985).
[21] M. Meyer, J.C. Mialocq, B. Perly. J. Phys. Chem. **94**, *1*, 98 (1990).
[22] K. Yagi, S. Shibata, T. Yano, A. Yasumori, M. Yamane, B. Dunn. J. Sol-Gel Sci. Technol. **4**, *1*, 67 (1995).
[23] E.Yu. Trofimova, D.A. Kurdyukov, S.A. Yakovlev, D.A. Kirilenko, Yu.A. Kukushkina, A.V. Nashchekin, A.A. Sitnikova, M.A. Yagovkina, V.G. Golubev. Nanotechnol. **24**, *15*, 155601 (2013).
[24] E.Yu. Trofimova, S.A. Grudinkin, Yu.A. Kukushkina, D.A. Kurdyukov, A.V. Medvedev, M.A. Yagovkina, V.G. Golubev. Phys. Solid State **54**, *6*, 1298 (2012).
[25] J.M.M. Hall, T. Reynolds, M.R. Henderson, N. Riesen, T.M. Monro, S. Afshar. Opt. Expr. **25**, *6*, 6192 (2017).
[26] A.A. Dukin, V.G. Golubev. Opt. Spectroscopy **130**, *13*, 2033 (2022).
[27] B. Valeur. Molecular Fluorescence: Principles and Applications. Wiley-VCH, Germany (2007). 381 p.
[28] T. Baumgärtel, C. von Borczyskowski, H. Graaf. Beilstein J. Nanotechnol. **4**, 218 (2013).
[29] A. Penzkofer, J. Wiedmann. Opt. Commun. **35**, *1*, 81 (1980).
[30] F. López Arbeloa, V. Martínez Martínez. Chem. Mater. **18**, *6*, 1407 (2006).
[31] A.A. Dukin, V.G. Golubev. Opt. Spectroscopy **130**, *11*, 1465 (2022).
[32] I. Gozhyk. PhD Thesis. École normale supérieure de Cachan, France (2012). 250 p.

Translated by E.Ilyinskaya